PERGAMON

Journal of Structural Geology 24 (2002) 323–338

JOURNAL OF STRUCTURAL GEOLOGY

www.elsevier.com/locate/jstrugeo

Polyphase hydrothermal breccias associated with unconformity-related uranium mineralization (Canada): from fractal analysis to structural significance

G. Lorilleux[a], M. Jébrak[b], M. Cuney[a,*], D. Baudemont[c]

[a]*CREGU-UMR G2R 7566, Université Henri Poincaré, BP 23, 54 501 Vandoeuvre-les-Nancy cedex, France*
[b]*UQÀM, Département des Sciences de la Terre et de l'Atmosphère, CP 8888, Montréal, Quebec, Canada H3C 3P8*
[c]*COGEMA Resources Inc, Exploration Department, 817-825 45th Street West, P.O. Box 9204, Saskatoon, SK, Canada S7K 3X5*

Received 24 May 2000; revised 8 May 2001; accepted 8 May 2001

Abstract

Sandstone-hosted breccias surrounding unconformity-related uranium ore in the Athabasca Basin, northern Saskatchewan, were mapped and described using drill core. Four main breccia types were distinguished and classified chronologically based on the type of matrix: microcrystalline quartz, sudoite–dravite, Fe–chlorite and polyphase carbonate. Mapping of the breccias has shown that they are controlled by various sets of basement faults, including a major graphite-rich structure. Breccia fragment morphologies were quantified using a fractal dimension analysis technique. The matrix percentage and the shape of the fragment morphometry distribution curve allow determination of the degree of maturity and the nature of fluid–rock interactions for each breccia. Microcrystalline quartz breccias are tectonic and fluid-assisted. Sudoite–dravite, Fe–chlorite and polyphase carbonate breccias were formed by dissolution of quartz. Mature sudoite–dravite and Fe–chlorite breccias have collapse textures formed, respectively, by dissolution opening and fluid-assisted brecciation. Breccias are the expression of basement fault reactivation postdating sandstone deposition (circa 1.7 Ga).

Each seismic event created structural conduits between variably pressured compartments, inducing fluid circulation from the basement to the sandstone. Fluids flowed more slowly in the strongly fractured sandstones and dissolved quartz to form solution breccias. Interaction of these basement-derived fluids with basinal fluids may have led to unconformity-related uranium mineralization deposition. This may explain the good correlation between breccia bodies and sandstone-hosted uranium ore, especially for the sudoite alteration event.

Keywords: Breccia; Fractal analysis; Uranium

1. Introduction

Breccias are commonly associated with hydrothermal ore deposits. Breccias occurring in mesothermal Au, Cu–Au–U Olympic Dam-type, low temperature F–Ba–Pb–Zn, epithermal Ag–Au and Mississippi Valley-type Zn–Pb deposits are well documented in literature (Jébrak, 1984; Laznicka, 1988; Reeve et al., 1990; Carrier and Jébrak, 1994; Genna et al., 1996; Sass-Gustkiewicz, 1996). Breccia formation has been discussed in particular by Phillips (1986), Sibson (1986), Laznicka (1988, 1989) and Jébrak (1992, 1997).

Numerous breccias have been described associated with the large unconformity-related uranium deposits of the Mesoproterozoic Athabasca basin (Saskatchewan, Canada) containing a resource of over 500,000 tonnes of uranium (Wheatley et al., 1996). These deposits are so-called because they are spatially related to the major unconformity underlying the Athabasca Basin. These breccias surround and locally host the high-grade unconformity-related uranium ores. They have been interpreted as being tectonic (Ey et al., 1985; Baudemont et al., 1993), meteor impact-related (Von Einsiedel, 1981; Harper, 1983; Ey, 1984; Pagel et al., 1985) and of dissolution-collapse origin (Wallis et al., 1983).

The significance of these breccias and their relation to faulting processes remain poorly known. The purpose of this study is to determine the mechanisms that led to the brecciation of the Athabasca sandstones, which host high-grade uranium deposits. A fractal analysis of fragment contours was carried out in order to quantify their shape complexity. The relationships between fault zones, hydrothermal breccias and uranium ore emplacement was

* Corresponding author. Tel.: +33-3-8391-2279; fax: +33-3-8391-3801.
E-mail address: michel.cuney@g2r.u-nancy.fr (M. Cuney).

0191-8141/01/$ - see front matter
PII: S0191-8141(01)00068-2

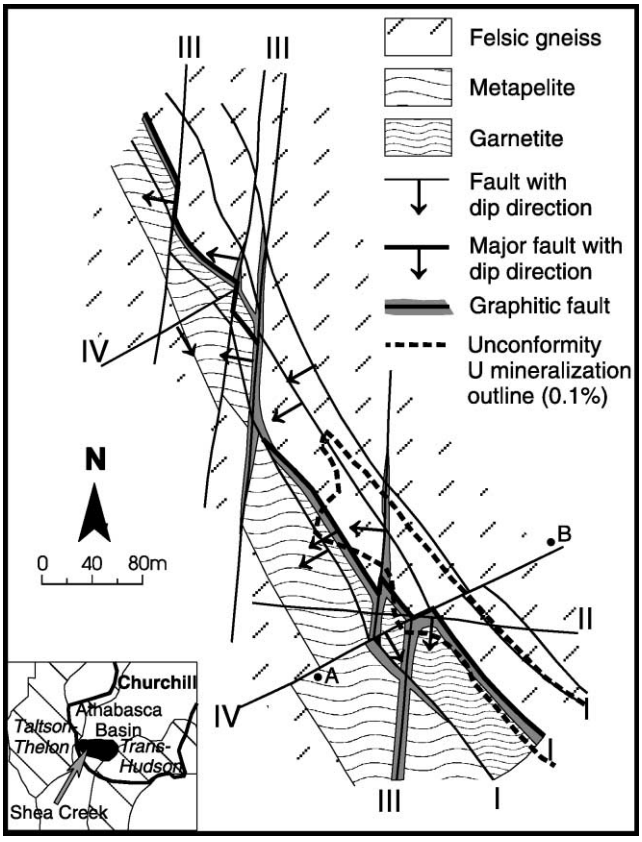

Fig. 1. Geological map of the study area in the south part of the Shea Creek exploration zone at 350 m below sea level (unconformity level). Felsic orthogneiss is the most widespread lithology and occurs on each side of a partly metasedimentary aluminous gneiss unit divided into metapelites and garnetites. Four types of faults are observed. The main Type I fault separates the metapelites from the felsic gneisses and is the main control of the uranium mineralization. Inset: location of the Shea Creek area and the Athabasca Basin relative to 2600–1800 Ma fold-thrust belts.

deciphered. Breccia-body geometry and chronological relationships were used to better understand the organization and functioning of faults in the sandstone basin. Simple textural and mineralogical characteristics of the Athabasca sandstone preclude the breccia features from being controlled by any compositional and structural anisotropy in the parent rocks.

Within the West Athabasca Basin, the Shea Creek exploration zone has been selected for a case study because of the extensive development of breccias, their variety and the dense exploration drilling pattern (20–40 m intervals between wells) in the south part, that allows a reconstruction of the 3D geometry of the breccia bodies, and extensive sampling possibilities (Fig. 1). The study area represents a zone of 600 m in length from north to south and 200 m in width.

2. Methodology

Breccias in the sandstones at Shea Creek were observed in cores of 45 mm in diameter. Detailed descriptions and drawings were made from both whole and sawn cores. The closely spaced drilling pattern allowed detailed mapping of structures and breccia bodies (Figs. 1–3). The samples were sawn along the core axis and high resolution close-up pictures of the planar sections were taken. The pictures were then scanned at 600 dpi resolution in gray levels. The contrast of the resulting images was then improved using Adobe Photoshop v. 3.0 software in order to easily separate the fragments and matrix. In this paper, matrix means interfragmental space that includes both microfragments and cement. Image analysis of the fragments was then performed on a computer using the public domain NIH-Image program developed at the U.S. National Institute of Health. The euclidian distance mapping (EDM) method was used to calculate the fractal dimensions of the fragment morphologies (Fig. 4) (Bérubé and Jébrak, 1999). Stripes of increasing thickness were computed from the particle outline. Then the log of the area of each stripe was plotted against the log of its thickness. The fractal dimension (D) was derived from the slope of the plot (s) using the relationship:

$$D = 2 - s \quad (1)$$

As the EDM method is not accurate for small fragment sizes, only fragment images with areas greater than 10,000 pixels were measured. For such fragments, the uncertainty for the EDM method is ± 0.01. A minimum of 24 fragments were used to obtain significant fragment morphometry distribution (FMD) curves (Fig. 5). EDM allows high precision fractal analysis and an amplified fractal dimension D^* was used instead of D, with:

$$D^* = (D - 1) \times 100 \quad (2)$$

Petrography of the samples was studied, with emphasis on textural and chronological relationships between the fragments and matrix. The fragments from unconsolidated breccias were mechanically removed and cleaned in water by ultrasonic waves. They were then dried and coated with carbon for scanning electron microscope (SEM) studies (Hitachi S-2500 SEM, Henri Poincaré University, Nancy, France). For comparison, non brecciated sandstones, sampled both in the vicinity and far from the U mineralization, were processed using the same methods. We used the terminology of Burley and Kantorowicz (1986) for dissolution textures of fragment surfaces observed under a SEM: pits and notches are typically 1–2 μm in size, embayments are about 20 microns and depressions are greater than 20 microns.

The breccia cement was analyzed by X-ray diffraction (XRD). On each sample analyzed, XRD patterns were determined on the less than 2-micron fractions on oriented aggregates in the range of 35–3 Å. On randomly oriented mineral powders, a range of 1.56–1.48 Å was used in order to distinguish di- or/and trioctahedral structures of clay minerals. XRD patterns were acquired by ERM (Études Recherches

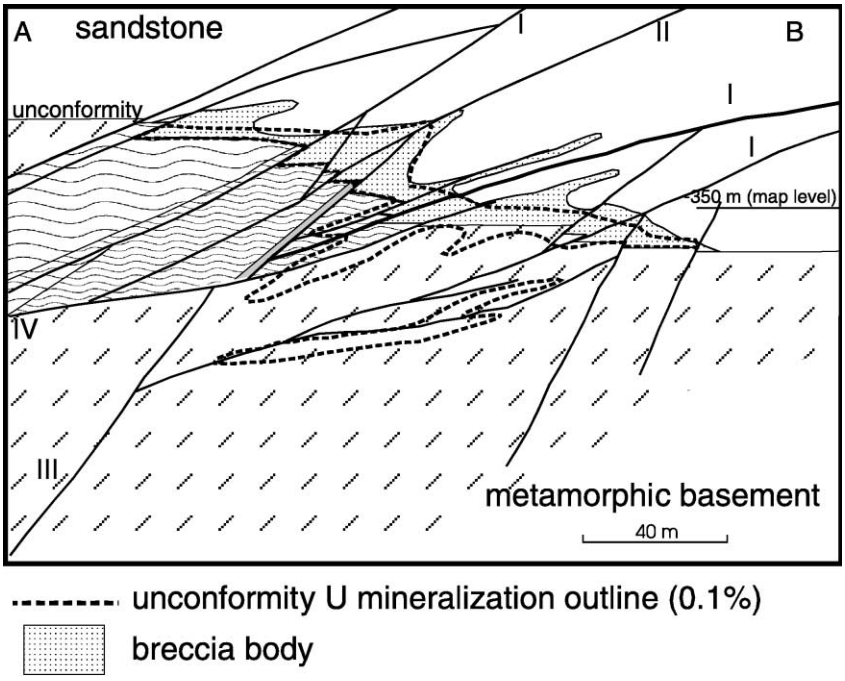

Fig. 2. Cross-section A–B displaying the relationships between the four types of faults, the breccia body, the unconformity and the mineralization. The breccia body includes all the breccia types observed in sandstones. The faults crosscut the unconformity and control the location of ore as well as the breccia body architecture. The lithology legend is the same as for Fig. 1.

Matériaux) in Poitiers (France) on a Siemens Kristalloflex D501 diffractometer (radiation: CuKα), equipped with an X-ray fluorescence detector (Si(Li) diode).

3. Geological setting

The Athabasca Basin lies within the southwest part of the Churchill Structural Province, between the Thelon–Taltson orogenic front (2.0–1.76 Ga; Ross and Eaton, 1997) to the west and the Trans-Hudson Orogen (1.88–1.76 Ga; Chiarenzelli et al., 1998) to the east (Fig. 1). The Shea Creek area is located in the western part of the Basin in the Western Craton, which represents a Lower Proterozoic stable cratonic foreland (Hoeve et al., 1980).

The Athabasca Basin formed during the Mesoproterozoic at about 1.7 Ga (Armstrong and Ramaekers, 1985; Kotzer et al., 1992) and is separated from the underlying basement by a major unconformity. It is composed of a series of sub-basins oriented NE–SW and controlled by faults rooted in the crystalline basement. The Athabasca Group is composed of thick, unmetamorphosed and flat-lying sequences of fluviatile to marine quartzose sandstones deposited in a land-proximal shelf environment (Ramaekers, 1981). A maximum total thickness of 4–5 km of sediments in the Basin has been proposed, based on fluid inclusions and diagenetic clay assemblages studies (Pagel, 1975; Hoeve et al., 1981; Halter, 1988).

At Shea Creek, the uneroded sandstone cover is about 700 m thick. The sandstones hosting the studied breccias mainly belong to the Manitou Falls C Formation, which directly overlies the basement at Shea Creek. They are typically medium to very coarse grained. Rare bedded clay layers are generally 1–2 cm thick. In non-mineralized zones, clay typically forms 0.5–15% of the rock and averages around 5% (Ramaekers, 1990). Major sandstone cements are quartz syntaxial overgrowths, clay minerals (kaolinite, illite, chlorite) and iron oxides.

Two main Paleoproterozoic basement lithostratigraphic units are found at Shea Creek: a metasedimentary unit in which graphite is mainly concentrated in faults, and a meta-igneous felsic gneiss unit (Fig. 1).

Four types of faults have been recognized, based on their orientation and movement (Table 1). They occur both in the Paleoproterozoic basement and in the Mesoproterozoic cover. Type I reverse faults are regional and oriented N130–150°. They are described in greater detail below. Type II fault structures are local and oriented N100–110°. They display late stage normal-sinistral movements with throws up to 10 m. Type III reverse faults are regional and oriented N5–15°. Like Type I faults, they are graphite-rich and have a ductile pre-Athabasca history. Their post-Athabasca throws may reach 20 m. Type IV fault structures are local and oriented N50–60°. They display sinistral-reverse to dextral-normal movements with throws of up to 10 m.

In the basement, the N130–150° Type I faults are ductile to brittle, 3–5 m wide and represented by graphite- and clay-rich gouges as well as numerous graphite-rich slip planes, parallel to the lithology and foliation. Several nearly

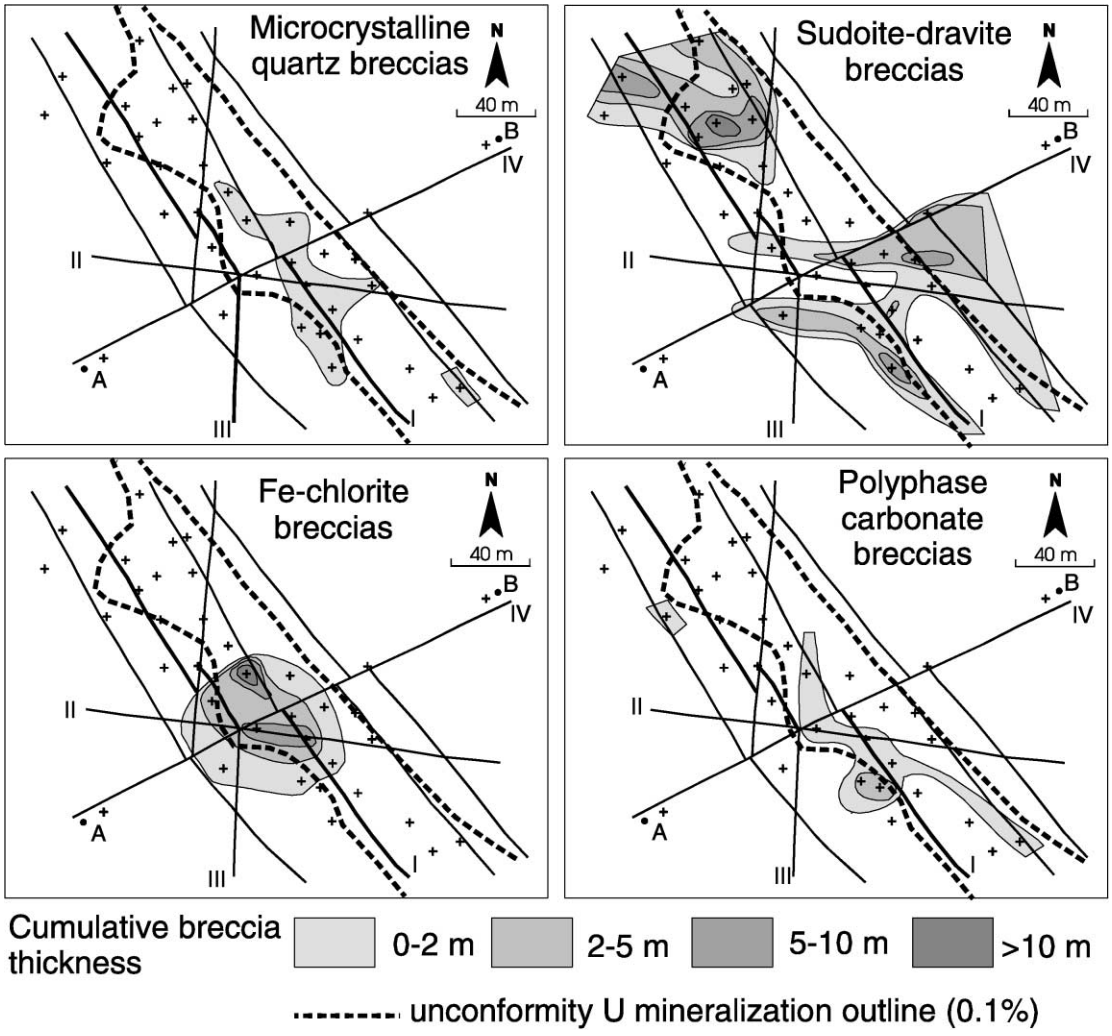

Fig. 3. Cumulative thickness of the different breccia types within 100 m of sandstones just above the unconformity projected on a structural map of the southern part of the Shea Creek area at 350 m below sea level (unconformity level, see Fig. 2). Black crosses represent drill holes intersecting the unconformity.

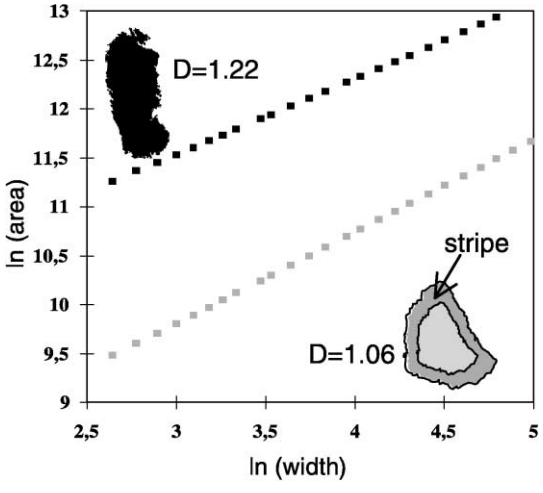

Fig. 4. The fractal dimension D of the particle morphology is computed using the Euclidean distance mapping method (Bérubé and Jébrak, 1999). Stripes of increasing thickness are computed from the particle outline. The log of the area of each stripe is then plotted against the log of their thickness. Measurement of two fragments from a polyphase carbonate breccia (black squares) and a sudoite–dravite breccia (gray squares) at Shea Creek.

parallel Type I faults are grouped into a fault zone up to 80 m wide (Figs. 1 and 2). Type I faults have produced several basement wedges with individual throws of up to 8 m at the unconformity (Fig. 2). A maximum cumulative post-Athabasca throw of 35 m is observed between points A and B at the unconformity (Figs. 1 and 2). In the sandstone, a large Type I fault is represented by a widely fractured zone (10–25 m wide).

These four fault types are associated with breccia bodies and alteration haloes in the sandstones. The alteration haloes mainly correspond to silicification and chloritization and are vertically more extensive than the breccias (up to more than 50 m above the unconformity). Within the alteration haloes, dilational veins have different mineralogical compositions that include quartz, chlorite, dravite, carbonates and pitchblende.

The high-grade uranium ore is found as massive pitchblende veins or impregnations reaching down to 40 m into the basement, and into the sandstone up to 40 m above the unconformity. The main ore pod is located at the

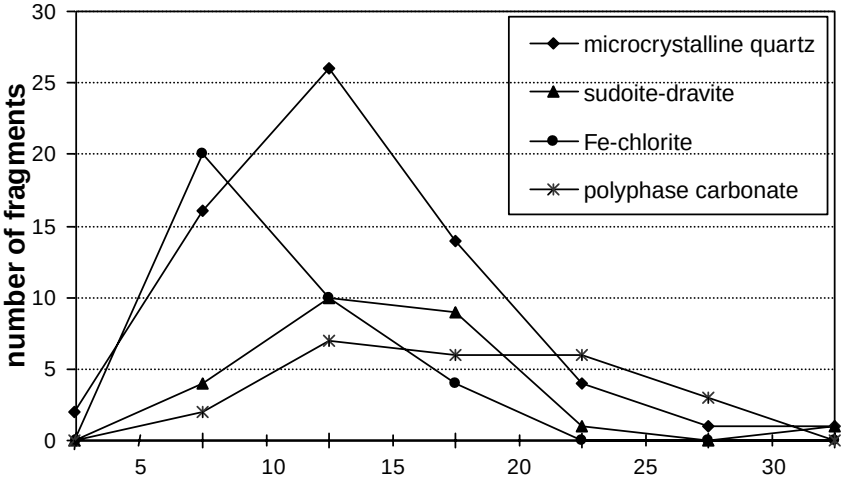

Fig. 5. Fragment morphology (D^*) distribution for the four types of breccias studied.

unconformity and is partly controlled by Type I faults and parallel low-angle dipping tension gashes (Figs. 1 and 2).

4. Description and mechanisms of formation of the breccias

Breccia fragment morphology and visually determined composition of the cements were used for breccia descriptions in the field. The nature of the cement made it possible to distinguish the different breccia types, whereas the fragment morphology and matrix proportion were used to describe the temporal and spatial breccia evolution within each particular type. Each breccia was characterized in terms of evolutionary maturity (Laznicka, 1988). An immature breccia has a low matrix proportion, typically about 20–30 vol.%, and weakly corroded and/or abraded and rarely rotated fragments. As the breccia evolves towards a more mature stage, the matrix proportion increases and the fragments become more corroded and/or abraded and rotated. Extreme maturity may be characterized by a decrease of the matrix proportion when collapse occurs.

Four main types of breccias, based on the assemblage of hydrothermal minerals, were recognized in the sandstone at Shea Creek: microcrystalline quartz, sudoite–dravite, Fe–chlorite and polyphase carbonate breccias (Table 2).

4.1. Microcrystalline quartz breccias

4.1.1. Description

Microcrystalline quartz breccias are characterized by white fine-grained quartz-rich matrix. The breccia body is spatially correlated with the main Type I fault (Fig. 3).

In hand specimen, textural variations are related to the maturity of the breccias (Table 2 and Fig. 6a). Immature breccias are represented by an oriented network of white microcrystalline quartz granulation seams or bands. They locally present jigsaw textures. The breccia contacts are typically fracture-controlled with variable dips. Offsets of

Table 1
Summary of the main characteristics of the four types of faults

Fault	Type I	Type II	Type III	Type IV
Importance	Regional	Local	Regional	Local
Azimuth	N130–150°	N100–110°	N5–15°	N50–60°
Dip	20–40°W	50–70°N	50–70°W	60–80°S
Post-Athabasca movements	Reverse	Normal-sinistral	Reverse	Sinistral-reverse to dextral-normal
Post-Athabasca horizontal offset	0 m	15–100 m	0 m	30 m
Post-Athabasca vertical offset	5–10 m (35 m for the fault zone)	2–10 m	10–20 m	10 m
Width in basement	3–5 m	1–10 m	3–5 m	3–5 m
Width in sandstone	10–25 m	1–15 m	20 m	20 m
Characteristics in basement	Graphite-rich and foliation-parallel	No graphite	Graphite-rich and foliation drag folding	No graphite
Style	Ductile-brittle with brittle reactivations	Brittle	Ductile-brittle with brittle reactivations	Brittle

Table 2
Summary of the main characteristics of the four types of breccias

Breccia body	Microcrystalline quartz	Sudoite–dravite	Fe–chlorite	Polyphase carbonate
Main structural control (order of decreasing importance)	Type I	Types I and II	Intersection of Types I, II and IV	Types I, II and III
Lateral extension	120 m	150 m	80 m	150 m
Vertical extension in sandstones	35 m	35 m	25 m	10 m
Maximum thickness	2 m	Few decimeters to several meters	Few decimeters up to 10–15 m	5 m
Fragments				
Variety	Homolithologic	Homolithologic	Homolithologic to heterolithologic (mature)	Homolithologic to heterolithologic
Alteration	Locally silicified	Locally silicified and rarely chloritized	Silicified and chloritized	Silicified, chloritized and hematized
Orientation	Yes	Rare	Yes when immature	No
Shape	Elongated	Variable and locally ovoïd	Elongated for immature breccias to variable	Complex
Roundness	Angular	Angular to rounded (more rounded when mature)	Angular to rounded	Angular to rounded
Size	1 mm to several centimeters	1 mm to several centimeters with tilted blocks	1 mm to several centimeters with tilted blocks	1 mm to several centimeters
Rotation	Rare	Common	Yes when mature	Common
Surface SEM textures	Not studied	Etching pits and embayments	Pits and notches mainly and few embayments and depressions	Not studied
Matrix				
Nature	Quartz	Detrital quartz ± sudoite and dravite	Detrital quartz + Fe–chlorite + Fe–kaolinite	Detrital quartz and siderite–chlorite
Quartz type	Microfragments or newly formed cement	Corroded detrital grains	Corroded detrital grains and angular microfragments	Corroded detrital grains
Microscopic quartz textures	Clean cusps	Dissolution cusps and gulfs	Dissolution cusps and gulfs	Dissolution cusps and gulfs
% matrix	20–60%	20–60%	20–70%	40–90%
Texture	Jigsaw when immature	Some fragment-supported when mature	Jigsaw when immature; fragment-supported when mature	Jigsaw (rare) when immature
Contacts	Fracture planes	Fracture planes to irregular	Fracture planes to irregular	Fracture planes to irregular

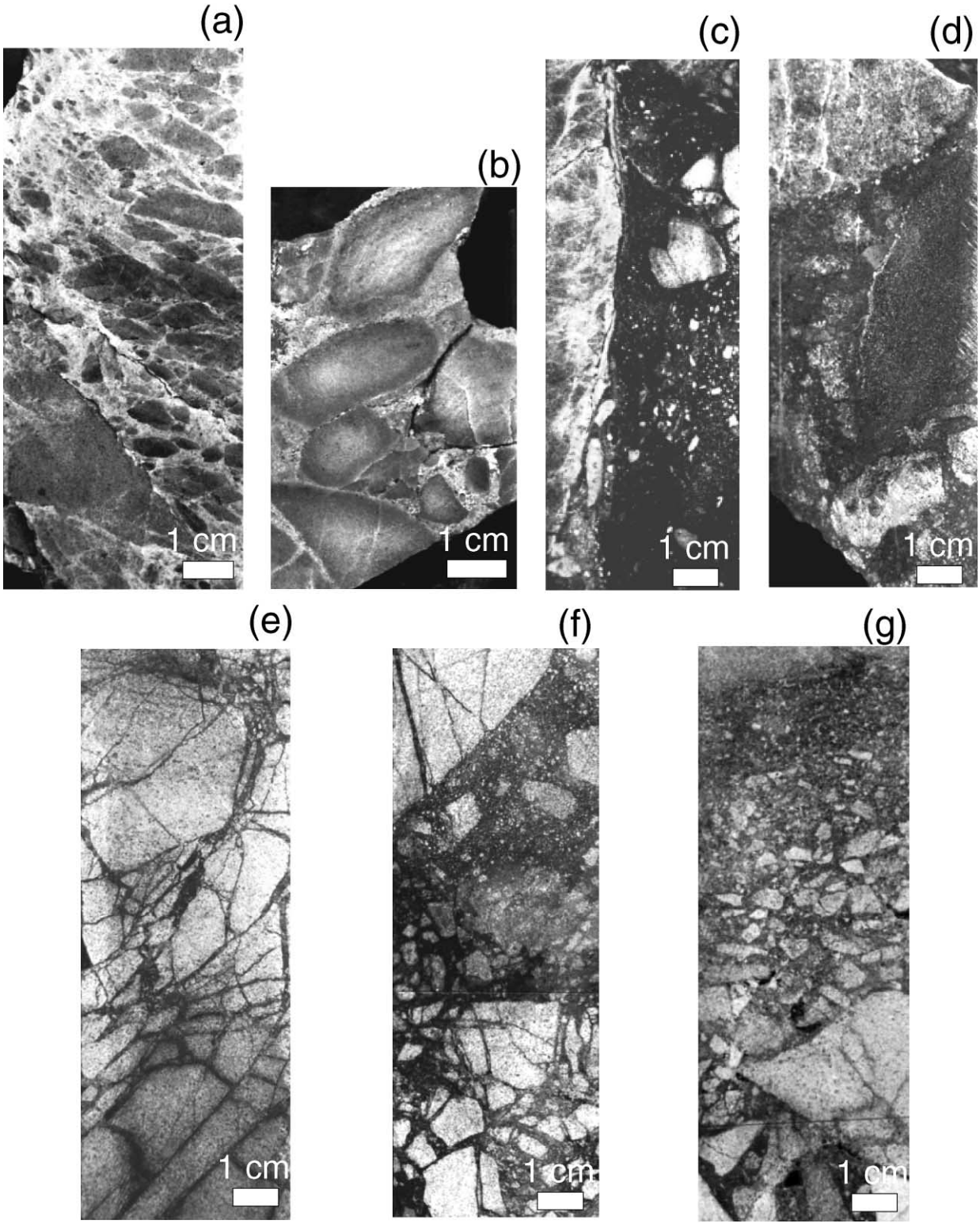

Fig. 6. Photographs illustrating the different types of fragment morphologies and the different textures. (a) Orientation of the fragments and anastomosing deformation bands and quartz-filled fractures in a microcrystalline quartz breccia. (b) Well rounded fragments with reaction rims in a sudoite–dravite breccia. (c) Fragment (on the left) of a microcrystalline quartz breccia in a Fe–chlorite breccia. (d) Complex fragment shapes in a polyphase carbonate breccia. The dark zone on the right is a sandstone ghost-fragment replaced by carbonate and hematite. Sequence (e)–(g) shows evolution from an immature to a mature Fe–chlorite breccia. Note the strong fracturing in the immature stage and the increase of matrix proportion, the corrosion of fragments and their reorganization into a graded bedding in the mature stage.

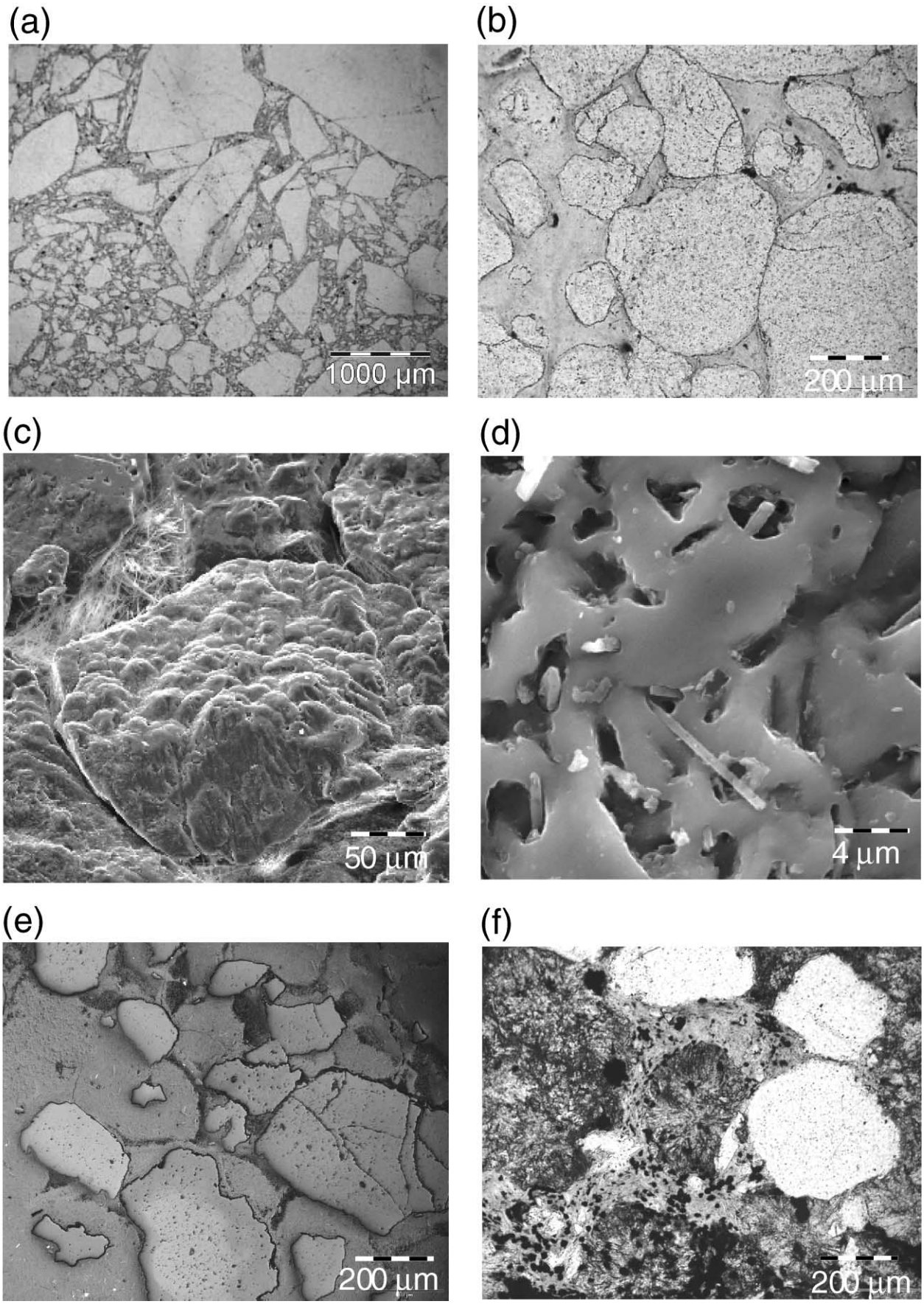
(a)
1000 µm
(b)
200 µm
(c)
50 µm
(d)
4 µm
(e)
200 µm
(f)
200 µm

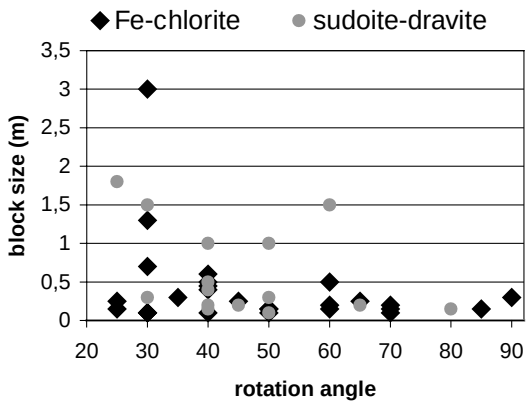

Fig. 8. Diagram showing the relationship between rotation angle and size of tilted blocks in sudoite–dravite and Fe–chlorite breccias. Rotation angle tends to increase as the size decreases.

1 mm to several centimeters are sometimes visible along granulation seams.

The matrix displays either microfragments of detrital quartz (Fig. 7a) or neogenic microcrystalline quartz cement. Quartz microfragments are often angular, locally oriented and sometimes elongated in splinters. They show clean cusps under SEM and are probably of mechanical origin. Consequently, the white fine-grained matrix is either attributable to the presence of microcrystalline quartz or to the fine granulation of the original detrital quartz grains and overgrowths. Jigsaw textures are locally recognized at the grain scale.

4.1.2. Interpretation

Oriented granulation seams in immature microcrystalline quartz breccias express tectonic deformation (Pittman, 1981; Antonellini and Aydin, 1994). The high matrix proportion of mature breccias is related to a strong increase in the spatial density of the deformation bands as well as a probable increase of the displacement. Local jigsaw textures and quartz fillings indicate fluid-assisted fracturing associated with tectonic movements. Angular fragments of sandstone and quartz microfragments (Fig. 7a) show that movements were not sufficient to round them. Therefore, microcrystalline quartz breccias were produced by fluid-assisted tectonic fracturing and microfaulting.

D^* values vary between 2.5 and 32.5 with a median at 12.5 Fig. 5; they are globally lower than those for the polyphase carbonate and sudoite–dravite breccia types, whose medians are, respectively, 17.5 and 13.5. This relatively low value is related to the presence of non-corroded angular fragments. The values between 22.5 and 32.5 are related to a late corrosion event observed on numerous samples.

4.2. Sudoite–dravite breccias

4.2.1. Description

Sudoite–dravite breccias are characterized by a matrix containing mainly detrital quartz grains and a very low proportion of white to light green cement.

Sudoite–dravite breccias compose the external zone of a coeval sudoite-rich breccia body centered on the unconformity-related U mineralization. Sudoite–dravite breccias are mainly controlled by Type II and I faults (Fig. 3).

Immature breccias have oriented, non-rotated and weakly corroded fragments. Fragment borders are controlled by fractures, which are themselves locally controlled by sandstone bedding. Mature breccias have non-oriented, locally rotated and rounded fragments and the proportion of matrix is up to 60 vol.%. Rounded fragments may show reaction rims (Fig. 6b). Most of the D^* values of the fragments are between 2.5 and 22.5, with a median of 13.5 (Fig. 5).

Fragment-supported textures with horizontally oriented fragments have been locally observed in mature breccias. Some tilted blocks, a few decimeters to more than 1 m wide, are locally found between breccias. The rotation angle tends to increase when size decreases (Fig. 8).

At a microscopic scale, fragment edges are rarely sharp and are often irregular and corroded. Within the fragments, detrital quartz grains with diagenetic overgrowths are corroded by sudoite and hydrothermal dravite. The matrix is usually composed of corroded quartz grains cemented by either dravite, or sudoite associated with dravite (Fig. 7b). Illite is locally present as revealed by XRD patterns. The global proportion of quartz grains in the matrix is greater than 85%. Grains are commonly in contact, frequently interlocked (pressure solution), but dissolution in the matrix is more intense than within the fragments.

4.2.2. Interpretation

As breccias evolve towards a mature stage, fragments become rounded. D^* values are low, with a median value of 13.5. The existence of well-rounded and non-rotated fragments indicates that the rounding is of chemical rather than mechanical origin. The presence of reaction rims on the borders of fragments and the corrosion textures of the quartz grains in the matrix confirm the chemical origin of these breccias (Figs. 6b and 7b). This evolution shows that quartz

Fig. 7. Photographs illustrating different microscopic textures of the breccias. (a) Non-oriented quartz clasts in the matrix of a microcrystalline quartz breccia (transmitted light). (b) Corroded detrital quartz grains in a sudoite- and dravite-rich cement within the matrix of a sudoite–dravite breccia (transmitted light). (c) Secondary electron SEM image of a corroded detrital quartz grain at the surface of a Fe–chlorite breccia fragment. Note the numerous dissolution pits and embayments. The white needle-shaped minerals between quartz grains are dravite. (d) Secondary electron SEM image of dissolution textures on a quartz grain. Note the corrosion pits and the dravite needles that are also corroded. (e) Corrosion textures of detrital quartz grains in the matrix of a Fe–chlorite breccia (reflected light). Note the hematite rims showing the location of the grain borders prior to the dissolution. (f) Corroded detrital quartz grains in a cement of chlorite and siderite nodules of a polyphase carbonate breccia.

dissolution propagated from the original fractures. Consequently, they are called solution breccias.

Local fragment-supported textures and horizontally oriented fragments in mature breccias probably indicate a collapse phenomenon. A temporary loss of cohesion of the breccia may occur when the amount of dissolved material becomes very large, inducing gravity control of the fragment organization (Knipe, 1993). This would explain the relationship between the rotation angle and size of the tilted blocks observed in mature breccias (Fig. 8).

4.3. Fe–chlorite breccias

4.3.1. Description

In hand specimen, Fe–chlorite breccias are characterized by a dark green to olive green clay-rich matrix (Fig. 6c and e–g). They may be slightly U mineralized. Fe–chlorite breccias form an 80-m-wide body controlled by the intersection of the main Type I fault with a Type II fault (Fig. 3). They are rooted at the unconformity where they are at their maximum. In upper sections they appear to follow the geometry of the Type I and II faults.

These breccia bodies usually correspond to alternating breccia units and tilted blocks of sandstone. In the core, tilted blocks may exceed 1 m in height and are considered to be breccia megafragments. The rotation angle of fragments generally increases as size decreases (Fig. 8).

Immature Fe–chlorite breccias have rather angular, slightly corroded and elongated fragments. They are often oriented and rarely rotated (Fig. 6e). Jigsaw textures are common with local dilation ratios (matrix/fragment volume ratios) greater than one.

Mature breccias have between 30 and 70 vol.% matrix and are locally heterolithic. Fragments in heterolithic breccias show different types or degree of silicification and chloritization. They have variable shapes and are rarely oriented and commonly rotated. Both angular and corroded fragments may coexist (Fig. 6g). D^* values vary between 2.5 and 22.5, with a median at 9, indicative of angular and weakly corroded fragments (Fig. 5).

Textures in mature breccias are matrix to fragment-supported. In the case of fragment-supported breccias, the fragments are rotated and there is a high proportion of angular fragments. Graded bedding is locally observed in the upper part of fragment-supported breccia units (Fig. 6g).

At a microscopic scale, the outline of angular and weakly corroded fragments described above is sharp and cross-cuts indistinct detrital grains and authigenic quartz. In corroded fragments, clay minerals have developed within corrosion cusps of detrital quartz grains, quartz overgrowths and quartz idiomorphic crystals (Table 2 and Fig. 7c and d). The transition between the fragments and the matrix is more progressive than for angular fragments.

The matrix is usually composed of quartz grains (from nearly 0 to more than 60 vol.%) in a cement. Quartz grains are both corroded detrital grains, displaying complex shapes (Fig. 7e) and angular microfragments. The proportion of the latter locally varies from 0 to about 50%. Corroded euhedral quartz crystals are also locally present. The cement is composed of Fe–chlorite mixed with Fe-rich kaolinite, smectite and variable proportions of dravite according to microscopic observations and XRD. Locally, fragments of sudoite mixed with dravite are also observed. Some late siderite crystals are present in shrinkage cracks formed in smectite.

Uranium mineralization is present as pitchblende and coffinite replacing and corroding idiomorphic pyrite disseminated within the clay matrix.

4.3.2. Interpretation

The existence of typical jigsaw textures in weakly corroded fragments is representative of hydraulic brecciation. However, the presence of corroded fragments and ubiquitous microscopic quartz dissolution textures indicate a chemical control of the breccia formation.

The evolution of a Fe–chlorite breccia from an immature to a mature stage is characterized by a displacement and mixing of angular and corroded fragments. Fragment-supported textures and graded bedding, and the relationship between rotation angle and size of tilted blocks in mature breccia zones indicate collapse phenomenon (Fig. 8). Such collapse events could explain the mixing of differently altered fragments.

4.4. Polyphase carbonate breccias

4.4.1. Description

Polyphase carbonate breccias typically display a red clay- and carbonate-rich matrix (Fig. 6d). They are locally associated with uranium mineralization. The body geometry of these breccias is controlled by the main Type I fault and Type II and III faults (Table 2 and Fig. 3). Their bodies are narrower than the other types of breccias and are located close to the unconformity.

Rare immature breccias have sub-angular fragments with a low matrix proportion and jigsaw textures. Mature breccias are commonly heterolithic and contain fragments of variably silicified, chloritized, hematized and carbonate-rich sandstone and of hematized and argillized basement fragments. They are matrix-supported and contain mostly rounded and corroded fragments. D^* values, from 2.5 to 32.5 with a median at 17.5 (Fig. 5), are globally higher than for the other types of breccias and reflect more complex fragment morphologies.

Matrix proportion varies between 40 and 90 vol.%. In the matrix, a greater percentage of quartz grains is sometimes found close to the edges of the fragments over a distance of a few millimeters, indicative of a corroded fragment rim. Locally, quartz grain distribution in the matrix is oriented within a fragment outline. Such distribution may then represent the bedding of an original sandstone fragment, replaced by hematite and carbonates (Fig. 6d).

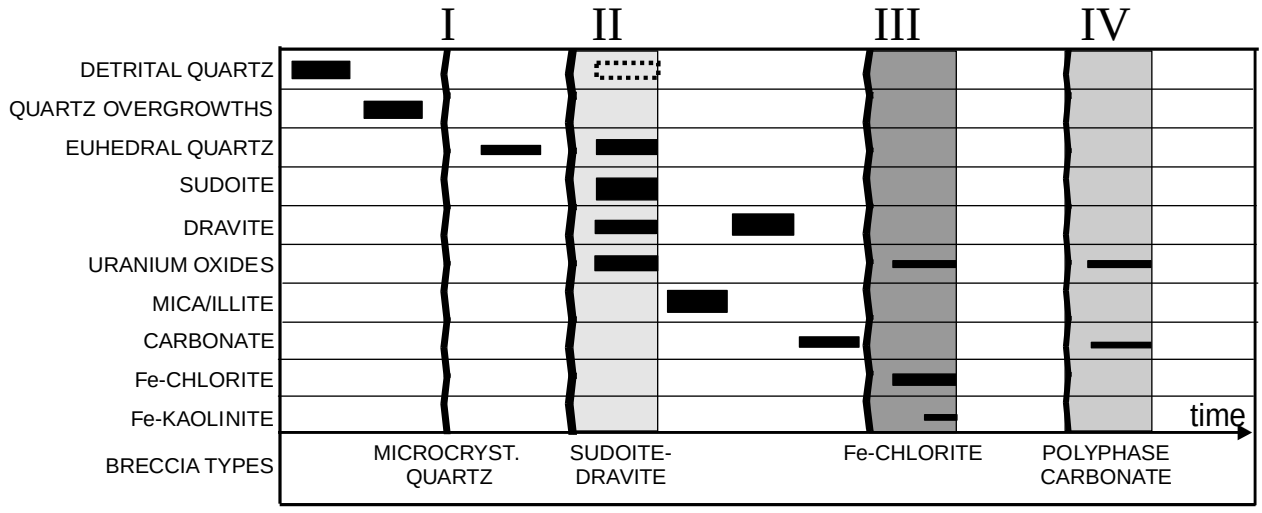

Fig. 9. Simplified paragenetic diagram showing chronological relationships between the four breccia varieties. Wavy lines = tectonic reactivations initiating fluid circulation, shaded areas = subsequent solution breccias, black rectangles = precipitation, empty dashed rectangle = dissolution.

At microscopic scale, sandstone fragments display corrosion of detrital quartz grains and their overgrowths by carbonates. The matrix is usually composed of corroded quartz grains (from 5 to 40 vol.%) in a cement of chlorite, illite and siderite (Fig. 7f). Siderite crystallized as spherulites. Very fine hematite disseminations give the rock a red color. Jigsaw textures are locally observed between fractured quartz grains within the matrix. Some corroded euhedral quartz crystals are also present.

4.4.2. Interpretation

Jigsaw textures in immature polyphase carbonate breccias and their remnants in more mature breccias indicate the existence of a possible early hydraulic fracturing event. This event is strongly overprinted by quartz corrosion. The presence of basement fragments in some of the mature breccias could be related to the proximity of the unconformity, and to reverse Type I faults creating basement wedges in sandstones.

5. Discussion

5.1. Chronological relationships and tectonic history

Crosscutting relationships between breccias and replacement minerals within their cements are the main criteria used to establish chronological relationships. A simplified chronological diagram is presented in Fig. 9. The similar succession of uranium deposition events and mineral paragenesis in several uranium deposits of the Athabasca Basin allowed the use of geochronological data established in ore bodies other than Shea Creek (Fayek and Kyser, 1997).

Contacts between microcrystalline quartz and sudoite–dravite breccias indicate the progression of a sudoite–dravite corrosion front that has altered the microcrystalline quartz texture. Microcrystalline quartz breccias never contain fragments of other types of breccias, whereas fragments of microcrystalline quartz are locally isolated and corroded within a sudoite–dravite matrix. Therefore, microcrystalline quartz breccias are considered to be the product of the earliest breccia event. The sudoite–dravite paragenesis is assumed to be contemporaneous with the main primary uranium deposition, as observed in the Cigar Lake U-deposit (Pacquet and Weber, 1993). In most of the unconformity-related uranium deposits of the Athabasca Basin, the primary uraninite mineralization event was dated between 1.52 and 1.25 Ga (Lainé, 1985; Fayek and Kyser, 1997). Consequently, the microcrystalline quartz breccias formed between the induration of the basal sediments of the Athabasca Basin at approximately 1.7 Ga, and uraninite deposition at 1.52–1.25 Ga.

Microcrystalline quartz breccias are contemporaneous with a reactivation of the reverse Type I fault and could be the expression of a post-Thelon–Taltson orogenic readjustment event.

Sudoite–dravite breccias formed before Fe–chlorite breccias because fragments of sudoite–dravite breccias are observed within Fe–chlorite breccias. The relationship between sudoite and associated dravite is not clear. They might be contemporaneous as documented by Pacquet and Weber (1993) at Cigar Lake, but dravite might also be related to a later event. One of the several dravite events observed at Shea Creek is clearly later than the sudoite phase.

The second event of sudoite–dravite and sudoite breccia formation is associated with the reactivation of both Type I and II faults. The presence of shallow dipping pitchblende-filled tension gashes indicates reverse movement along the Type I faults. The contemporaneous formation of all the other unconformity-related uranium deposits in the western and eastern parts of the Athabasca Basin associated with

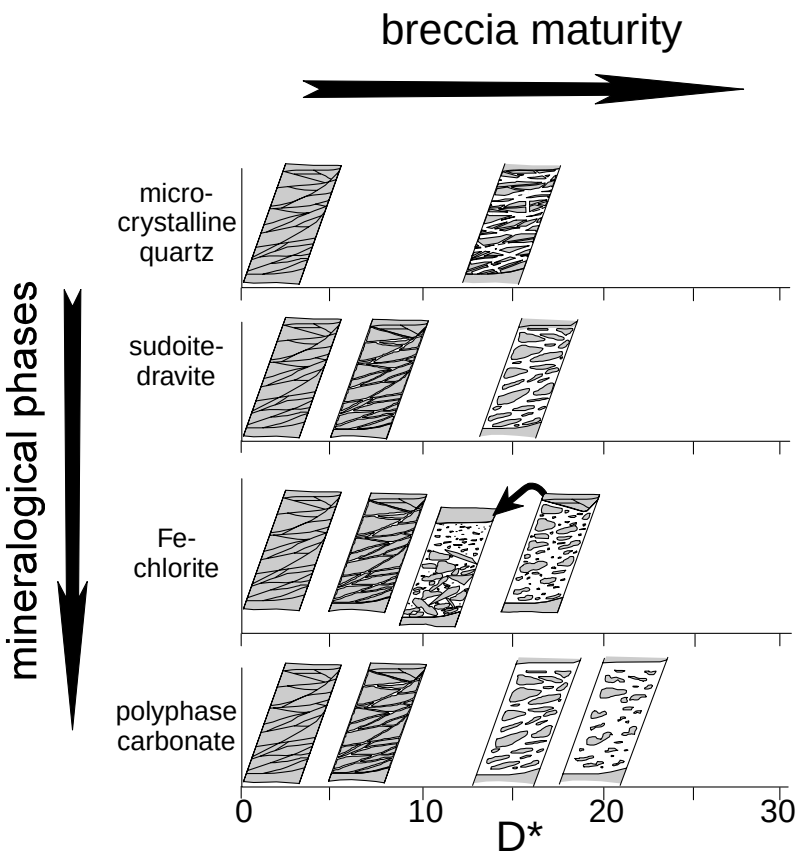

Fig. 10. Synthetic diagram showing the temporal evolution of each breccia type according to their main descriptive features and fragment morphometry measurements. Note the reverse evolution for the last stage of Fe–chlorite collapse breccias.

reverse faulting indicates that this is a compressional phase that occurred at least at the scale of the Athabasca Basin. The presence of almost undeformed Mackenzie diabase dikes crosscutting U-ore dated 1.27 Ga (Le Cheminant and Heaman, 1989) suggests that this phase occurred between the oldest dated U-mineralization (1.52 Ga) and 1.27 Ga.

Fe–chlorite breccia formation corresponds to a probable reactivation of Type II and/or IV faults with a composite strike- and dip-slip movement. It indicates a strong rotation of the regional stress field as the major Type I faults are not reactivated. Philippe et al. (1993) indicated a K–Ar age of 900 ± 50 Ma for the ferrikaolinite in perched bodies at Cigar Lake. The slightly mineralized Fe–chlorite breccias at Shea Creek, which contain Fe-rich kaolinite, might therefore be coeval with this phase. They could correspond to a regional uranium mineralization event or a remobilization phase dated at 918 and 860 Ma, at the Key Lake and Rabbit Lake unconformity-related deposits, respectively (Lainé, 1985).

Polyphase carbonate breccias contain chloritized fragments that are interpreted to correspond to sudoite–dravite breccia relicts. Siderite crystals occurring in cracks of the Fe–chlorite breccia matrix are assumed to be contemporaneous with the siderite present in the matrix of polyphase carbonate breccias. Consequently, polyphase carbonate breccias would be younger than the other types of breccias.

The polyphase carbonate breccia-forming event corresponds to the reactivation of the reverse Type I and Type II and III faults. These breccias could have formed between 300 and 200 Ma as indicated by dating of a pitchblende–carbonate association in the Dominique–Peter unconformity-related U deposit located in the western part of the Athabasca Basin (Bell, 1985). The existence of remobilized uranium mineralization dated at 290, 215 and 200 Ma, respectively, at Maurice Bay, Key Lake and Rabbit Lake deposits (Lainé, 1985), located in the east part of the Athabasca Basin, suggests that the event is also regional.

The four breccia bodies studied, therefore, are clearly related to regional tectonic events between 1.7 Ga and 200 Ma. However, more systematic age determinations would be necessary to ascertain the general validity of these ages. The control of the breccia bodies by different structural orientations indicates variations of the regional stress field between each seismic event.

5.2. Breccia maturation

The textural characteristics and the morphometric

measurements of the four types of breccias allow interpretation of each of them in terms of maturity (Fig. 10).

5.2.1. Immature breccias

Immature microcrystalline quartz breccia fragments are controlled by granulation seams and fluid-assisted quartz-filled fractures. The fracture intensity may vary in space according to the distance to the faults.

Immature sudoite–dravite breccias have fracture-controlled, weakly corroded and oriented fragments. Jigsaw textures indicate a fluid-assisted fracturing regime. Sudoite–dravite breccias are coeval with the primary uraninite mineralization event that probably coincided with a period of peak diagenesis under a 4–5-km-thick sedimentary pile (Pagel, 1975; Fayek and Kyser, 1997). This environment is consistent with the development of fluid-assisted fractures as fluid pressures in sedimentary basins below 3 km depths are commonly lithostatic (Egeberg, 1992; Hedenquist et al., 1992).

Therefore, the first stage of breccia formation is controlled by tectonic and fluid-assisted fractures, as indicated by fragment shapes and low values of D^* in immature breccias (Fig. 10).

5.2.2. Mature breccias

Fractal analysis of the fragment shapes allows recognition of both the intensity and type of corrosion processes, and also its kinetic component.

D^* median values for the four breccia types vary from 9 to 17.5, corresponding to different complexity levels of the fragment shapes (Fig. 5). For each breccia type, increasing D^* values indicate the evolution from an immature to a mature stage. This evolution is also characterized by an increase of the matrix proportion and by a loss of the original orientation of the fragments. In the case of microcrystalline quartz breccias, the maturation corresponds to a strong increase of fracturing intensity. Sudoite–dravite, Fe–chlorite and polyphase carbonate breccia maturation is mainly associated with quartz dissolution.

Fragment morphologies of solution breccias are controlled by the quartz consumption reaction. Two different regimes of the dissolution reaction may be distinguished (Hurst and Bjørkum, 1986; Sahimi and Tsotsis, 1987; Jébrak, 1997). In the diffusion-limited regime, only the most exposed part of the solid is reached and consumed as a reactant; corners will become smooth and fragments may ultimately take a spherical morphology, decreasing the fractal dimension. Such a process will occur if there is a strong chemical disequilibrium between the rock and the fluid. In the kinetic regime, the alteration–dissolution rate is limited only by the chemical reaction rate. The fluid has a relatively low chemical reactivity and the reaction will enhance the contrasting compositions of the fragments and create more complex shape contours. Increasing D^* values are therefore significant of an evolution from diffusion-limited to kinetic processes in quartz dissolution that indicates a decrease in hydrothermal solution undersaturation.

However, detailed analysis reveals a more complex history: in Fe–chlorite breccias, the observation of some complex shapes and pervasively altered fragments as well as the predominance of pits on fragment surfaces (Table 2 and Fig. 7d) would indicate local kinetic regimes (Burley and Kantorowicz, 1986). In sudoite–dravite breccias, the presence of rounded fragments is probably indicative of a diffusion-limited dissolution regime.

The FMD is indicative of the evolution of the corrosion process. Microcrystalline quartz breccias, sudoite–dravite and polyphase carbonate breccias display normal FMD that demonstrate homogeneous fragment shapes and a stationary process: the same D^* value for the different fragments within a type of breccia indicates that the same corrosion process has reached an equilibrium within the sandstone.

The distribution of D^* values (FMD) for Fe–chlorite breccias is not normal. This reflects the superimposition of the quartz dissolution process on another phenomenon. Low values represent non-corroded fragments fallen from the breccia hanging wall during the collapse event. Higher values would be representative of the fragments corroded by the dissolution event prior to the collapse.

The last stage of evolution of Fe–chlorite breccias is a collapse event. There are two possible origins for this collapse. The first hypothesis is a chemical origin. If more quartz is dissolved than new clay minerals are formed, cavities will appear and may enhance fluid flow and a positive feedback loop, resulting in further dissolution leading to cavity enlargement. If large enough, collapse could occur and produce graded-bedded and fragment-supported textures as well as a mixture of corroded and angular fragments. Similar textures were observed by Dzulynski and Sass-Gustkiewicz (1989) in solution-collapse breccias hosting Mississippi Valley-type deposits.

The second hypothesis is a fluid-assisted origin. The local presence of angular and very weakly corroded fragments organized in jigsaw textures suggest fluid-assisted brecciation. The corroded detrital quartz grains in the clay cement indicate that the dissolution occurred by fluid percolation along fractures before the hydraulic event causing the fall of detrital quartz grains into the matrix during the brecciation. The incorporation of non-corroded fragments coming from the breccia fractured walls during the collapse caused an inverse evolution of the breccia maturity (Fig. 10). This interpretation is the most probable as it explains all the features of the Fe–chlorite breccias.

Fluid-assisted brecciation may have been triggered by two different processes. The first process is permeability sealing by cementation above the quartz dissolution zones. This could have led to the formation of abnormally pressured compartments (Doligez et al., 1988) and subsequent hydraulic brecciation and collapse following the expansion phase. Even small amounts of secondary mineral

precipitation can dramatically affect the permeability in a granular media (Tenthorey et al., 1998). The second process is a tectonic movement, which could have interrupted the dissolution process and created openings and associated critical breccias (Jébrak, 1997).

Some collapse textures were also observed in the sudoite–dravite breccias. The absence of corroded and non-corroded fragment mixtures indicates rather minor collapse. The absence of jigsaw textures suggests a dissolution origin rather than a fluid-assisted origin.

Mature breccia fragment morphologies therefore reflect two types of breccia formation: fluid-assisted and solution. They represent, respectively, the physical and chemical aspects of fluid–rock interactions. Both fluid-assisted and solution types may occur as part of the evolution of the same breccia system as demonstrated by the Fe–chlorite breccias.

Consequently, maturity corresponds to the temporal evolution of breccias. Furthermore, spatial variations of fracture intensity at the immature stage also control the maturity as they induce permeability variations. Breccia maturity therefore varies both in space and time.

5.3. Fluid circulation and ore genesis

The spatial organization of breccia bodies suggests a strong control by faults. At the 400 m scale of the study area, the major Type I fault seems to be the principal control, but extended breccia bodies occur mostly at or close to fault intersections. The graphite enrichment in the basement of the major Type I fault could be responsible for its preferential reactivation during almost every seismic event because of the lubricating properties of graphite.

Analysis of mature breccias indicates that breccia development is controlled by fluid–rock interactions. Therefore, breccia-forming events in sandstone coincide with basement fault reactivation and subsequent onsets of fluid circulation favored by increased fracture permeability, especially at fault intersections. As the fluids were undersaturated relative to quartz, it is highly improbable that they came from the sandstones. They were probably derived from the basement along permeability channels such as the main graphite-rich Type I shear zone, or the cross-cutting high angle faults such as the Type II structures, or intersections of both (Kyser et al., 1989). Shear zones are proposed as conduits for focused flow of overpressured fluids (Kerrich and Allison, 1978; Robert et al., 1983; Ridley, 1993). At each seismic event, transient fluids would have moved rapidly along the basement channels (high pressure regime) and then would have slowed down in the strongly fractured sandstones (low pressure regime) above the unconformity.

Fluids, widely dispersed in the fractured zone, reacted with the local lithologies leading to breccia development. According to the genetic models of Hoeve et al. (1980) and Fayek and Kyser (1997), the fluids interacted with basinal fluids, leading to uranium ore deposition. The wide development of sudoite-rich breccias relative to other breccia bodies as well as the extent and high-grade of the U-mineralization suggest a major fluid circulation phase between 1.52 and 1.27 Ga.

The weak spatial correlation of sudoite–dravite breccias with uranium mineralization is attributable to their zoning relationship with coeval and extremely mature sudoite breccias that are closer to the unconformity and show good correlation with the U ore. Fe–chlorite and polyphase carbonate breccias also display a good correlation with U mineralization but are more local than the sudoite breccias.

6. Conclusion

Four breccia types have been distinguished in the sandstone surrounding unconformity-related uranium mineralization in the southern part of the Shea Creek area: microcrystalline quartz, sudoite–dravite, Fe–chlorite and polyphase carbonate breccias.

Their fragment morphologies have been quantified using fractal dimension analysis. The matrix percentage and the shape of the fragment morphometry distribution (FMD) curves have been used to determine the degree of maturity and the nature of fluid–rock interactions for each breccia. The fractal dimension increases with the degree of maturity.

Microcrystalline quartz breccias are tectonic and fluid-assisted. Their maturation corresponds to an increase of fracturing density. Sudoite–dravite, Fe–chlorite and polyphase carbonate breccias are solution breccias. Solution breccia maturation may be described in three phases. In the first phase, fault reactivation and fluid overpressure induced fracturing and fluid circulation. The second phase is characterized by quartz dissolution resulting from the chemical interaction of a basement-derived fluid with the overlying sandstones. Collapse may occur in a third phase due to fluid-assisted brecciation or dissolution opening and is exemplified by Fe–chlorite and sudoite–dravite breccias, respectively. Consequently, breccia development is the result of alternating physical and chemical fluid–rock interactions, with high and low rates, respectively. In the former case, breccia maturity evolution would represent spatial variations, whereas in the latter it would correspond to temporal variations.

The four breccia bodies are mainly controlled by reverse Type I faults and intersections with other types of faults. They are the expression of basement fault reactivations occurring between 1.7 Ga and 200 Ma. The first seismic reactivation could be the expression of minor readjustment movements following the Thelon–Taltson orogeny. The second deformational event between 1.52 and 1.27 Ga was a regional compressional phase leading to the main primary uranium mineralization. The third and fourth events could also have been regional as they are possibly contemporaneous with mineralization phases dated circa 900 Ma and

between 300 and 200 Ma, respectively, in several deposits. Different breccia body controls indicate major changes of the regional stress field with time.

Each seismic event created structural connections between variably pressured compartments, inducing fluid circulation from the basement to the sandstones. Fluids were slowed down in the widely fractured sandstones, giving them time to react with the quartz to form solution breccias. Interaction of these fluids with basin fluids may have led to unconformity-related uranium mineralization deposition. This may explain the good correlation of breccia bodies with the mineralization, especially for the sudoite event.

Acknowledgements

We are grateful to COGEMA and COGEMA Resources Inc. for their financial and technical support. More specifically, we would like to thank Patrice Bruneton and Ken Wheatley for helpful reviews, Philippe Portella for stimulating discussions and Jean-Claude Carisey for permission to publish the geological data collected in the field in June of 1999. The manuscript was improved by reviews from Peter Laznicka and Charlie Sammis.

References

Antonellini, M., Aydin, A., 1994. Effect of faulting on fluid flow in porous sandstones: petrophysical properties. American Association of Petroleum Geologists Bulletin 78, 355–377.

Armstrong, R.L., Ramaekers, P., 1985. Sr isotopic study of Helikian sediment and diabase dikes in the Athabasca Basin, northern Saskatchewan. Canadian Journal of Earth Sciences 22, 399–407.

Baudemont, D., Piquard, J.P., Ey, F., Zimmerman, J., 1993. The Sue Uranium Deposits, Saskatchewan, Canada. Exploration and Mining Geology 2, 179–202.

Bell, K., 1985. Geochronology of the Carswell area, Northern Saskatchewan. In: Lainé, R., Alonso, D., Svab, M. (Eds.). The Carswell Structure Uranium Deposits, Saskatchewan. Geological Association of Canada Special Paper 29, pp. 33–46.

Bérubé, D., Jébrak, M., 1999. High precision boundary fractal analysis for shape characterization. Computers & Geosciences 25, 1059–1071.

Burley, S.D., Kantorowicz, J.D., 1986. Thin section and S.E.M. textural criteria for the recognition of cement-dissolution porosity in sandstones. Sedimentology 33, 587–604.

Carrier, A., Jébrak, M., 1994. Structural evolution and metallogeny of the Silidor mesothermal gold–quartz deposit, southern Abitibi greenstone belt, Quebec. Geological Association of Canada — Mineralogical Association of Canada, Annual Meeting Abstracts, Waterloo. No. 19, A-18.

Chiarenzelli, J., Aspler, L., Villeneuve, M., Lewry, J., 1998. Early Proterozoic Evolution of the Saskatchewan Craton and its Allochthonous Cover, Trans-Hudson Orogen. Journal of Geology 106, 247–267.

Doligez, B., Burrus, J., Ungerer, P., 1988. Hydraulic fracturing during basin scale fluid migration: an integrated approach. In: Hitchon, B., Bachu, S. (Eds.). Fluid Flow, Heat Transfer and Mass Transport in Fractured Rocks. 4th Canadian/American Conference on Hydrogeology, pp. 251–259.

Dzulynski, S., Sass-Gustkiewicz, M., 1989. Pb–Zn ores. In: Bosák, P., Ford, D.C., Glazek, J., Horácek, I. (Eds.). Paleokarst. A Systematic and Regional Review. Elsevier and Academia, Amsterdam and Prana, pp. 377–396.

Egeberg, P.K., 1992. Brines in Sedimentary Environments. Academic Press, London.

von Einsiedel, C.A., 1981. Petrography and geochemistry of the Cluff Lake breccias, Carswell structure, Northern Saskatchewan. B.Sc. thesis, Carleton University, Ottawa, Ontario.

Ey, F., 1984. Un exemple de gisement d'uranium sous discordance: les minéralisations protérozoÏques de Cluff Lake, Saskatchewan, Canada. Thèse d'Etat, Université Louis Pasteur, Strasbourg.

Ey, F., Gauthier-Lafaye, F., Lillié, F., Weber, F., 1985. A uranium unconformity deposit: the geological setting of the D orebody (Saskatchewan-Canada). In: Lainé, R., Alonso, D., Svab, M. (Eds.). The Carswell Structure Uranium Deposits, Saskatchewan. Geological Association of Canada Special Paper 29, pp. 121–138.

Fayek, M., Kyser, T.K., 1997. Characterization of multiple fluid-flow events and Rare-Earth-Element mobility associated with formation of unconformity-type uranium deposits in the Athabasca Basin, Saskatchewan. The Canadian Mineralogist 35, 627–658.

Genna, A., Jébrak, M., Marcoux, E., Milési, J.P., 1996. Genesis of cockade breccias in the tectonic evolution of the Cirotan epithermal gold system, West Java. Canadian Journal of Earth Sciences 33, 93–102.

Halter, G., 1988. Zonalités des altérations dans l'environnement des gisements d'uranium associés à la discordance du Protérozoïque Moyen (Saskatchewan, Canada). Thèse de doctorat, Université Louis Pasteur, Strasbourg.

Harper, C.T., 1983. The geology and uranium deposits of the central part of the Carswell Structure, Northern Saskatchewan, Canada. Unpublished Ph.D. thesis, Colorado School of Mines, Golden, Colorado.

Hedenquist, J.W., Reyes, A.G., Simmons, S.F., Taguchi, S., 1992. The thermal and geochemical structure of geothermal and epithermal systems: a framework for interpreting fluid inclusion data. European Journal of Mineralogy 4, 989–1015.

Hoeve, J., Sibbald, T.I.I., Ramaekers, P., Lewry, J.F., 1980. Athabasca Basin unconformity-type uranium deposits: a special class of sandstone-type deposits?. In: Ferguson, S., Goleby, A. (Eds.). Uranium in the Pine Creek Geosyncline. International Atomic Energy Agency, Vienna, pp. 575–594.

Hoeve, J., Rawsthorn, K., Quirt, D., 1981. Uranium Metallogenetic Studies: Clay Mineral Stratigraphy and Diagenesis in the Athabasca Group. Saskatchewan Research Council Publication 22, pp. 76–89.

Hurst, A.R., Bjørkum, P.E., 1986. Discussion: thin section and S.E.M. textural criteria for the recognition of cement-dissolution porosity in sandstones. Sedimentology 33, 605–614.

Jébrak, M., 1984. Contribution à l'histoire naturelle des filons F–Ba des Hercynides françaises et marocaines. Thèse ès Sciences, Document Bureau de Recherches Géologiques et Minières 99.

Jébrak, M., 1992. Les textures intra-filoniennes, marqueurs des conditions hydrauliques et tectoniques. Chronique de la Recherche Minière 506, 25–35.

Jébrak, M., 1997. Hydrothermal breccias in vein-type ore deposits: a review of mechanisms, morphology and size distribution. Ore Geology Reviews 306, 1–24.

Kerrich, R., Allison, I., 1978. Vein geometry and hydrostatics during Yellowknife mineralization. Canadian Journal of Earth Sciences 15, 1653–1660.

Knipe, R.J., 1993. The influence of fault zone processes and diagenesis on fluid flow. In: Horbury, A.D., Robinson, A.G. (Eds.). Diagenesis and Basin Development. American Association of Petroleum Geologists. Studies in Geology 36, pp. 135–148.

Kotzer, T.G., Kyser, T.K., Irving, E., 1992. Paleomagnetism and the evolution of fluids in the Proterozoic Athabasca Basin, northern Saskatchewan, Canada. Canadian Journal of Earth Sciences 29, 1474–1491.

Kyser, T.K., Wilson, M.R., Ruhrmann, G., 1989. Stable isotope constraints

on the role of graphite in the genesis of unconformity-type uranium deposits. Canadian Journal of Earth Sciences 26, 490–498.

Lainé, R., 1985. The Carswell uranium deposits — an example of not so unique unconformity-related uranium mineralization. In: Lainé, R., Alonso, D., Svab, M. (Eds.). The Carswell Structure Uranium Deposits, Saskatchewan. Geological Association of Canada Special Paper 29, pp. 225–230.

Laznicka, P., 1988. Breccias and Coarse Fragmentites. Elsevier, Amsterdam Developments in Economic Geology, 25.

Laznicka, P., 1989. Breccias and ores. Part 1: history, organization and petrography of breccias. Ore Geology Reviews 4, 315–344.

Le Cheminant, A.N., Heaman, L.M., 1989. Mackenzie igneous events, Canada: Middle Proterozoic hotspot magmatism associated with ocean opening. Earth and Planetary Sciences Letters 96, 38–48.

Pacquet, A., Weber, F., 1993. Pétrographie et minéralogie des halos d'altération autour du gisement de Cigar Lake et leurs relations avec les minéralisations. Canadian Journal of Earth Sciences 30, 674–688.

Pagel, M., 1975. Détermination des conditions physico-chimiques de la silicification diagénétique des grès Athabasca (Canada) au moyen des inclusions fluides. Compte-rendu de l'Académie des Sciences 280, 2301–2304.

Pagel, M., Weatley, K., Ey, F., 1985. The origin of the Carswell circular structure. In: Lainé, R., Alonso, D., Svab, M. (Eds.). The Carswell Structure Uranium Deposits, Saskatchewan. Geological Association of Canada Special Paper 29, pp. 213–223.

Philippe, S., Lancelot, J.R., Clauer, N., Pacquet, A., 1993. Formation and evolution of the Cigar Lake uranium deposit based on U–Pb and K–Ar isotope systematics. Canadian Journal of Earth Sciences 30, 720–730.

Phillips, W.J., 1986. Hydraulic fracturing effects in the formation of mineral deposits. Institution of Mining and Metallurgy Transactions, section B: Applied Earth Science 95, B17–B24.

Pittman, E.D., 1981. Effect of fault-related granulation on porosity and permeability of quartz sandstones, Simpson Group (Ordovician), Oklahoma. American Association of Petroleum Geologists Bulletin 65, 2381–2387.

Ramaekers, P., 1981. Hudsonian and Helikian basins of the Athabasca region, Northern Saskatchewan. Geological Survey of Canada Paper 81, 219–233.

Ramaekers, P., 1990. Geology of the Athabasca Group (Helikian) in Northern Saskatchewan. Saskatchewan Energy and Mines, Saskatchewan Geological Survey, Report 195.

Reeve, J.S., Cross, K.C., Smith, R.N., Oreskes, N., 1990. Olympic Dam. Copper–uranium–gold–silver deposit. In: Hughes, E.E. (Ed.). Geology of the Mineral Deposits of Australia and Papua New Guinea. The Australasian Institute of Mining and Metallurgy, Melbourne, pp. 1009–1035.

Ridley, J., 1993. The relations between mean rock stress and fluid flow in the crust: with reference to vein- and lode-style gold deposits. Ore Geology Reviews 8, 23–37.

Robert, F., Brown, A.C., Audet, A.J., 1983. Structural control of gold mineralization at the Sigma Mine, Val d'Or, Québec. Canadian Institute of Mining, Metallurgy and Petroleum Bulletin 76, 72–80.

Ross, G.M., Eaton, D.W., 1997. Winagami reflection sequence: seismic evidence for postcollisional magmatism in the Proterozoic of western Canada. Geology 25, 199–202.

Sahimi, M., Tsotsis, T.T., 1987. Dynamic scaling for the fragmentation of reactive porous media. Physical Review Letters 59, 888–891.

Sass-Gustkiewicz, M., 1996. Internal sediments as a key to understanding the hydrothermal karst origin of the Upper Silesian Zn–Pb ore deposits. Society of Economic Geologists Special Publication 4, pp. 171–181

Sibson, R.H., 1986. Brecciation processes in fault zones: inferences from earthquake rupturing. Pure and Applied Geophysics 124, 161–175.

Tenthorey, E., Scholz, C.H., Aharonov, E., Léger, A., 1998. Precipitation sealing and diagenesis. 1. Experimental results. Journal of Geophysical Research 103, 23951–23967.

Wallis, R.H., Saracoglu, N., Brummer, J.J., Golightly, J.P., 1983. Geology of the McLean uranium deposits. In: Cameron, E.M. (Ed.). Uranium Exploration in Athabasca Basin, Saskatchewan, Canada. Saskatchewan Energy and Mines, Geological Survey of Canada, pp. 71–110.

Wheatley, K., Murphy, J., Leppin, M., Cutts, C., Climie, J.A., 1996. Advances in the genetic model and exploration techniques for unconformity type uranium deposits in the Athabasca basin. Canadian Institute of Mining, Metallurgy and Petroleum (CIM) Conference, Edmonton, Alberta, May 1996.